metals

MDPI

Article

Unveiling High-Pressure Behavior of Sc_3AlC MAX Phase: A Comprehensive Theoretical Study on Structural, Mechanical, Dislocation, and Electronic Properties

Junping Xi [1,*], Zhipeng Wang [2,*], Linkun Zhang [3], Li Ma [4] and Pingying Tang [4]

[1] Department of Mechanical and Automotive Engineering, Science and Technology College of Hubei University of Arts and Science, Xiangyang 441025, China
[2] State Key Laboratory of Advanced Design and Manufacturing Technology for Vehicle, Hunan University, Changsha 410082, China
[3] State Key Laboratory for Powder Metallurgy, Central South University, Changsha 410083, China
[4] Guangxi Key Laboratory of Functional Information Materials and Intelligent Information Processing, Nanning Normal University, Nanning 530001, China
* Correspondence: xjphndx@163.com (J.X.); wzp1205@hnu.edu.cn (Z.W.)

Abstract: The structural, mechanical, dislocation, and electronic properties of the Sc_3AlC MAX phase under applied pressure are investigated in detail using first-principles calculations. Key parameters, including lattice parameter ratios, elastic constants, Young's modulus, bulk modulus, shear modulus, brittle-to-ductile behavior, Poisson's ratio, anisotropy, Cauchy pressure, yield strength, Vickers hardness, and energy factors, are systematically analyzed as a function of applied pressure. The results demonstrate that the Sc_3AlC MAX phase exhibits remarkable mechanical stability within the pressure range of 0 to 60 GPa. Notably, applied pressure markedly improves its mechanical properties, such as resistance to elastic, bulk, and shear deformations. The *B/G* ratio suggests a tendency toward ductile behavior with increasing pressure, and the negative Cauchy pressure indicates the directional characteristics of interatomic bonding in nature. Vickers hardness and yield strength increase under pressures of 0 to 10 GPa and then decrease sharply above 50 GPa. High pressure suppresses dislocation nucleation due to the increased energy factors, along with twinning deformation. Furthermore, electronic structure analysis confirms that high pressure enhances the interatomic bonding in the Sc_3AlC MAX phase, while the enhancement effect is not substantial. This study offers critical insights for designing MAX phase materials for extreme environments, advancing applications in aerospace and electronics fields.

Keywords: MAX phase; first-principles calculations; mechanical properties; energy factor; high pressure

Academic Editor: Sónia Simões

Received: 22 March 2025
Revised: 20 April 2025
Accepted: 25 April 2025
Published: 27 April 2025

Citation: Xi, J.; Wang, Z.; Zhang, L.; Ma, L.; Tang, P. Unveiling High-Pressure Behavior of Sc_3AlC MAX Phase: A Comprehensive Theoretical Study on Structural, Mechanical, Dislocation, and Electronic Properties. *Metals* **2025**, *15*, 492. https://doi.org/10.3390/met15050492

1. Introduction

Ceramic materials are valued for their high hardness, as well as excellent corrosion and oxidation resistance. Nevertheless, their inherent brittleness restricts their use in structural applications. On the other hand, metallic materials exhibit superior toughness despite inherently inferior corrosion and oxidation resistance [1,2]. In order to combine the advantages of both, a class of materials known as cermets has emerged. Specifically, MAX-phase ceramics (transition metal carbides/nitrides) have attracted significant attention due to their unique layered atomic structure and an exceptional combination of physicochemical properties. As a result, these materials synergistically integrate high hardness and strength

with excellent electrical conductivity and thermal stability, thereby positioning them as promising candidates for diverse advanced engineering applications [3,4]. Furthermore, MAX phases exhibit outstanding plasticity at elevated temperatures, alongside high fracture toughness, thermal shock resistance, and stiffness. Consequently, these attributes render them suitable for applications in high-temperature components, wear-resistant coatings, and corrosion-resistant systems [5–9].

As a typical MAX-phase cermet, Sc_3AlC exhibits unique performance advantages, especially in the aerospace industry. Owing to its high specific strength, excellent oxidation resistance, and superior corrosion resistance [10,11], Sc_3AlC is well-suited for manufacturing high-performance aerospace engine components (e.g., engine components under hypersonic flight loads), as well as structural materials for aircraft. In the field of electronics, the semiconductor properties and outstanding electrical performance of Sc_3AlC [12] facilitate its application in the development of advanced electronic devices, including field-effect transistors and solar cells, thereby driving advancements in electronic technology. Compared to mainstream materials, such as titanium alloys (e.g., Ti-6Al-4V) and nickel-based superalloys in aerospace, or silicon and gallium arsenide in electronics, Sc_3AlC offers distinct advantages. Titanium alloys provide excellent strength-to-weight ratios but suffer from inferior oxidation resistance at high temperatures, requiring protective coatings that increase costs and complexity. Nickel-based superalloys, while robust at high temperatures, are denser and less corrosion-resistant in harsh environments. Sc_3AlC, with a density comparable to titanium alloys (~4.5 g/cm^3) and superior oxidation resistance, reduces the need for coatings and enhances durability in oxidative environments [10,11]. In electronics, silicon is cost-effective but lacks the mechanical robustness of Sc_3AlC, which can integrate structural and functional roles in next-generation devices. Other MAX phases, such as Ti_2AlC or Ti_3AlC_2 [9], share similar advantages but may have lower specific strength or electrical conductivity compared to Sc_3AlC due to differences in composition and bonding [4,6]. Despite its promising properties, the widescale implementation of Sc_3AlC faces several obstacles, primarily the high cost and limited availability of scandium, which is a rare and expensive element compared to titanium or other transition metals used in MAX phases like Ti_2AlC or Ti_3AlC_2 [9]. Synthesis challenges also pose barriers, as producing high-purity Sc_3AlC requires precise control to avoid defects or impurities that could degrade its mechanical and electrical properties. Additionally, scalable manufacturing processes, such as cost-effective powder metallurgy or additive manufacturing, are not yet fully optimized for scandium-based MAX phases, limiting their commercial viability [3]. However, recent progress is addressing these challenges. Advances in synthesis techniques, such as spark plasma sintering and reactive hot pressing, have improved the quality and affordability of MAX phases like Ti_3SiC_2 and Ti_2AlC, which are now used in applications such as turbine blades, heat exchangers, and protective coatings [3,9]. Similar methods have been successfully applied to Sc_3AlC, with recent studies reporting high-purity synthesis via reactive sintering at reduced temperatures, enhancing feasibility for industrial-scale production [12]. These developments, coupled with the growing industrial adoption of other MAX phases in aerospace, suggest a promising trajectory for Sc_3AlC in high-value applications.

Currently, research on Sc_3AlC MAX-phase materials has made significant progress. From a structural perspective, both experimental studies and theoretical calculations have confirmed that its crystal structure is of the anti-perovskite type, with a space group of *Pm-3m* [13–15]. Nevertheless, research on Sc_3AlC under high-pressure conditions is still limited. Owing to limitations in high-pressure experimental techniques, the available data on its mechanical properties and electronic structure evolution under extreme pressure are scarce, thereby hindering the acquisition of comprehensive and precise information. Consequently, current studies are still constrained in fully elucidating the complex effects of high pressure

on its structural stability and electronic characteristics. Several critical scientific issues require further investigation. These include systematic investigation of the evolution of mechanical properties, particularly the variation of elastic modulus and yield strength under high pressure; exploration of the mechanisms by which high pressure influences its electronic structure, including changes in band structure and electronic density of states; and analysis of the phase transition behavior of Sc_3AlC under extreme conditions and its impact on overall performance. Therefore, this study aims to systematically investigate the structural, mechanical, dislocation, and electronic properties of the Sc_3AlC MAX phase under high pressure. Addressing these critical issues will not only contribute to a deeper understanding of the high-pressure behavior of the Sc_3AlC MAX phase, but also provide valuable guidance for extreme environment applications.

2. Methodology

First-principles calculations based on density functional theory (DFT) are executed using the Vienna ab initio Simulation Package (VASP) [16,17] to systematically investigate the electronic structure and mechanical properties of Sc_3AlC. The ion-electron interactions are modeled using the Projected Augmented-Wave (PAW) method [18] to ensure accurate electronic structure modeling. The generalized gradient approximation (GGA) with the Perdew-Burke-Ernzerhof (PBE) functional is adopted to describe the exchange-correlation potential [19]. The calculations, performed within the DFT framework, utilize a cubic Sc_3AlC structure (space group *Pm-3m*). A plane-wave basis set with a kinetic energy cutoff of 550 eV is applied to expand the electronic wavefunctions. The Brillouin zone is sampled using an $11 \times 11 \times 11$ Γ-centered *k*-point mesh to ensure high-precision *k*-space integration [20]. Convergence criteria are set to 0.01 eV/Å for atomic forces and 10^{-6} eV/atom for total energy. To evaluate pressure-dependent behavior, applied pressures range from 0 to 60 GPa. Total energy calculations under compressive strains are conducted to assess mechanical properties and high-pressure stability. The electronic structure is evaluated through density of states (DOS) calculation. The results are employed to examine element-specific contributions (Sc, Al, C) to the electronic structure. The electronic configurations—Sc ($3d^1$ $4s^2$), Al ($3s^2$ $3p^1$), and C ($1s^2$ $2s^2$ $2p^2$)—critically influence bonding characteristics and material stability. Figure 1 depicts the cubic crystal structure of the Sc_3AlC unit cell.

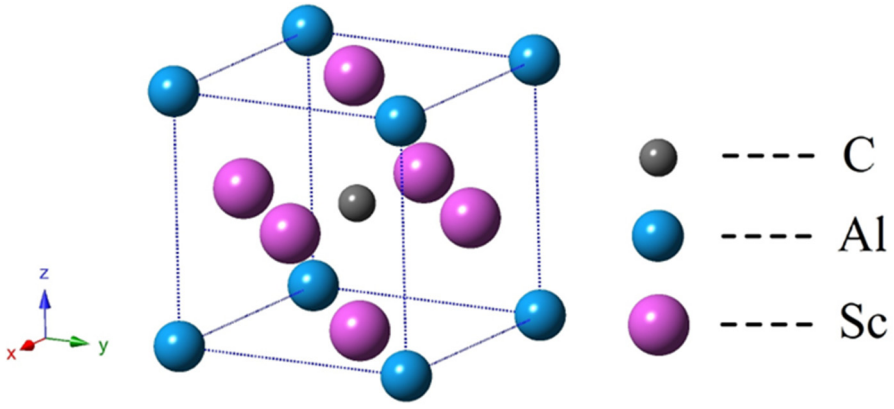

Figure 1. Structural model of Sc_3AlC MAX phase with $a_0 = 4.500$ Å.

3. Results and Discussions

3.1. Structure Properties and Stability

The equilibrium crystal structure of Sc_3AlC in the MAX phase is determined through first-principles calculations. The total energy-volume dependence is characterized using the Birch-Murnaghan equation of state [21], providing a precise description of energy

variations as a function of volume. The equilibrium volume is evaluated by systematically varying the volume from 0.9 V_0 to 1.1 V_0, where V_0 denotes the equilibrium volume under the condition of $P = 0$ and $T = 0$. Figure 2 demonstrates that the structure reaches its minimum total energy ($E_t = -34.548438$ eV) at an equilibrium volume of $V_0 = 91.13$ Å^3. The equilibrium lattice constant (a_0) is calculated as 4.500 Å. These results are derived under the condition of $P = 0$ and $T = 0$, confirming that the calculated values reflect the ideal equilibrium structure of Sc_3AlC in the MAX phase. Table 1 illustrates that the calculated results show good agreement with prior experimental and theoretical studies [10,12,22–27].

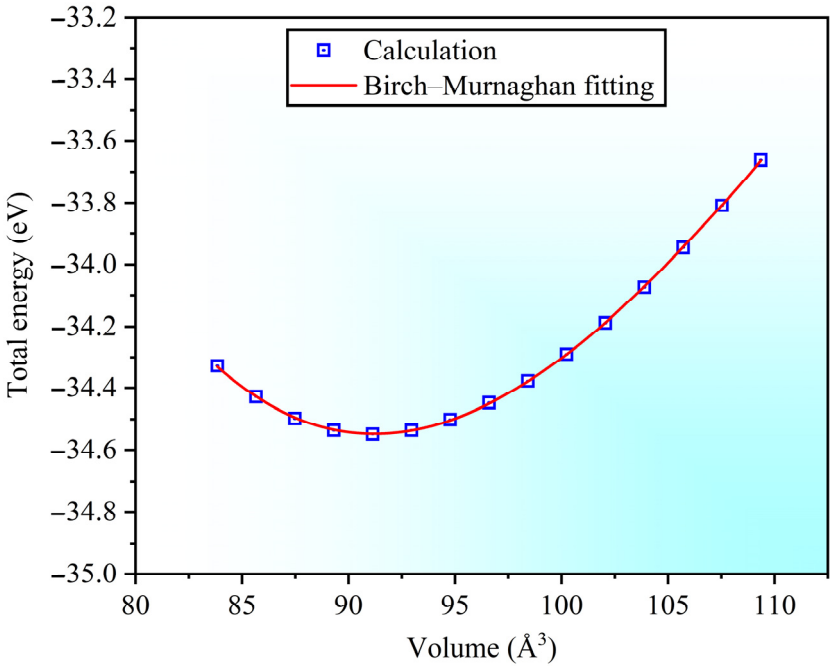

Figure 2. The correlation between total energy and unit cell volume.

Table 1. Lattice parameter of Sc_3AlC MAX phase compared with experimental and theoretical values.

Sc_3AlC	Present	Experimental Values	Theoretical Values
Lattice parameter	4.500	4.498 [22], 4.48 [10], 4.5004 [12]	4.508 [26], 4.480 [25], 4.508 [23], 4.51 [27], 4.51 [24], 4.5119 [12]

To further investigate the effect of high pressure on the crystal structure of Sc_3AlC, this study conducts a series of systematic structural optimization calculations under different pressure conditions, accurately determining the equilibrium lattice constant and volume of Sc_3AlC within the pressure range of 0 to 60 GPa. The corresponding trends are shown in Figure 3. It is clearly observed that as the pressure increases from 0 to 60 GPa, both the lattice constant ratio a/a_0 and the volume ratio V/V_0 exhibit a decreasing trend. This indicates that under high pressure, the interatomic distances within Sc_3AlC continuously decrease, leading to a denser atomic arrangement and enhanced electron interactions.

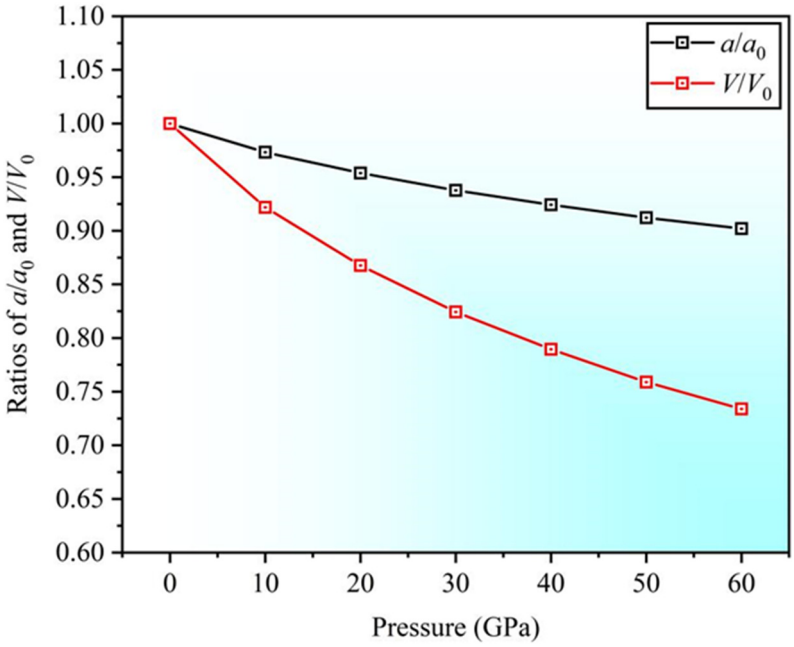

Figure 3. Variation curves depicting V/V_0 and a/a_0 ratios versus applied pressure.

In anisotropic materials, structural stability is intrinsically linked to elastic constants C_{ij}, which indicate the material's ability to resist elastic deformation. Elastic constants C_{ij} not only characterize the material's response to external stresses but also highlight directional variations in mechanical properties. For cubic crystals, especially under high-pressure or large-strain conditions, elastic constants (C_{11}, C_{12}, and C_{44}) are critical in determining the material's resistance to stress-induced deformation. In solid-state physics, the stability of cubic crystals is primarily evaluated based on their elastic constants [28–30]. The stability criteria are defined by specific conditions related to elastic constants, ensuring that the crystal remains stable under diverse external stresses.

$$(C_{11} - C_{12}) > 0, C_{11} > 0, C_{44} > 0, (C_{11} + 2C_{12}) > 0 \quad (1)$$

The computational results obtained in this study demonstrate strong agreement with previous theoretical calculations reported in references [22–27], as evidenced by the comparative analysis presented in Table 2. This consistency between our findings and established theoretical frameworks not only corroborates the validity of our computational approach but also reinforces the reliability and precision of the current research methodology.

Table 2. Calculated results compared with other theoretical data at T = 0 and P = 0 (Unit: GPa).

Sc_3AlC	Present	Theoretical Data
C_{11}	235.2	220.85 [26], 224.90 [25], 219.20 [23], 220 [24], 225 [27], 220 [22]
C_{12}	45.21	42.15 [26], 40.50 [25], 40.35 [23], 40 [24], 41.5 [27], 43 [22]
C_{44}	80.08	80.12 [26], 80.80 [25], 80.19 [23], 79 [24], 80.3 [27], 79 [22]
B	108.54	101.72 [26], 101.60 [25], 99.98 [23], 99.91 [24], 102.70 [27], 102 [22]
E	203.62	197.03 [26], 199.70 [25], 196.40 [23], 195 [24], 199.27 [27]
G	85.74	83.69 [26], 85.10 [25], 83.80 [23], 83.26 [24], 84.68 [27], 83 [22]
σ	0.16	0.18 [26], 0.17 [25], 0.17 [23], 0.17 [24], 0.18 [27], 0.18 [22]

To explore the effect of high pressure on the elastic properties of Sc_3AlC, the elastic constants are calculated in the pressures range of 0 to 60 GPa. Figure 4 depicts the variation of elastic constants (C_{11}, C_{12}, and C_{44}) as a function of pressure. As pressure increases

from 0 to 60 GPa, the elastic constants exhibit a monotonic increase, rising steadily from their initial values. This behavior indicates that Sc_3AlC maintains structural stability under high pressure. Notably, these elastic constants fulfill the stability criterion defined by Equation (1). The results demonstrate that Sc_3AlC retains structural stability under high pressure and exhibits enhanced resistance to structural phase transitions.

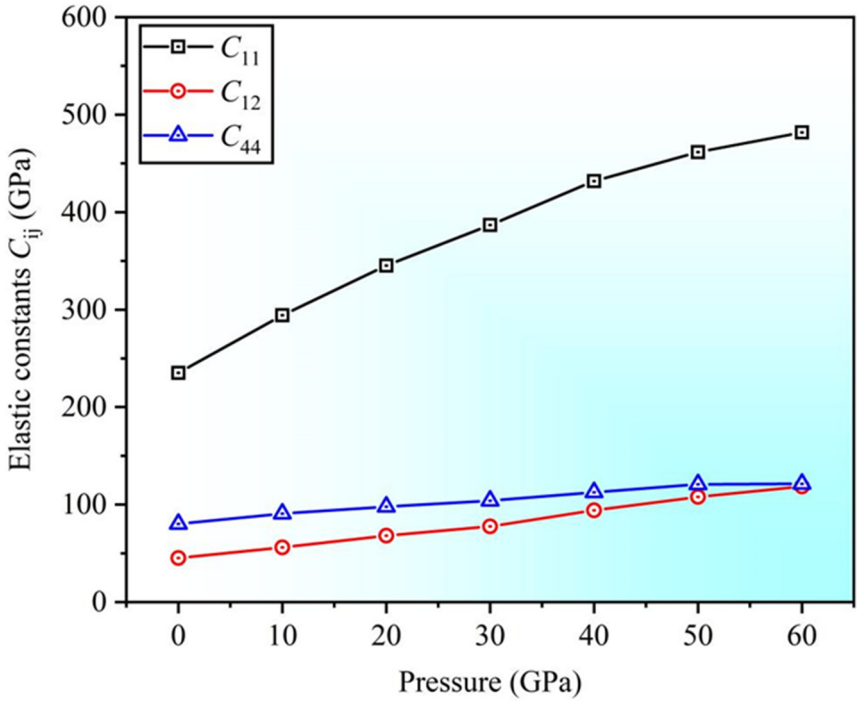

Figure 4. Variation curves depicting elastic constants C_{ij} versus applied pressure.

3.2. Mechanical Properties

The moduli of materials, including bulk modulus B, Young's modulus E, and shear modulus G, play a crucial role in evaluating mechanical properties [31,32]. The magnitude of these moduli is directly related to the material's strength. Materials with high modulus usually have high strength, indicating that they can maintain their shape and resist deformation under external stresses. The Voigt-Reuss-Hill (VRH) method is a commonly used approach to calculate the effective moduli of composite or anisotropic materials [33,34], as with the Equations (2)–(4). It can be used to estimate the relationships between different moduli (such as bulk modulus, Young's modulus, and shear modulus), contributing to evaluate the material's performance under varying stress and deformation conditions. Table 2 presents the computed moduli and compares them with previous studies.

$$B = \frac{1}{3}(C_{11} + 2C_{12}) \tag{2}$$

$$G = \frac{1}{2}(G_V + G_R) \tag{3}$$

$$E = \frac{9BG}{3B + G} \tag{4}$$

In the aforementioned equations, G_V and G_R represent Voigt and Reuss shear modulus, respectively, which are mathematically expressed by Equations (5) and (6):

$$G_V = \frac{(C_{11} - C_{12} + 3C_{44})}{5} \tag{5}$$

$$G_R = \frac{5(C_{11} - C_{12})C_{44}}{4C_{44} + 3(C_{11} - C_{12})} \quad (6)$$

Figure 5 illustrates the variations of bulk modulus (*B*), Young's modulus (*E*), and shear modulus (*G*) within the pressure range of 0 to 60 GPa. As the pressure increases from 0 to 60 GPa, the bulk modulus (*B*), Young's modulus (*E*), and shear modulus (*G*) all exhibit an upward trend. The increase in Young's modulus (*E*) is the most significant, gradually rising from its initial value to considerably higher values. This indicates that under high pressure, the ability of Sc_3AlC to resist elastic deformation is significantly enhanced, and the atomic bonding strength increases substantially as pressure increases. The bulk modulus (*B*) also increases steadily, reflecting the gradual enhancement of the ability of Sc_3AlC to resist uniform compression under high-pressure conditions, indicating that the internal structural stability of the crystal improves as the pressure increases. The shear modulus (*G*) also increases with pressure, although the rate of change is more moderate compared to Young's modulus (*E*) and bulk modulus (*B*), suggesting that under high pressure, the ability of Sc_3AlC to resist shear deformation improves, although the rate of change is more moderate. These trends in moduli suggest that the mechanical properties of Sc_3AlC are reinforced under high-pressure conditions.

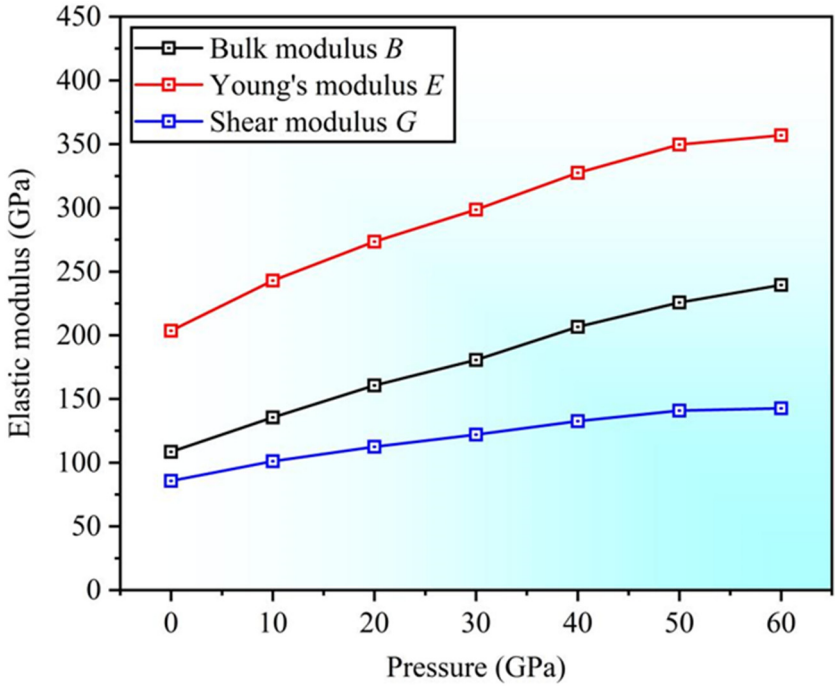

Figure 5. Variation curves depicting Young's modulus, bulk modulus, and shear modulus versus applied pressure.

The brittle-to-ductile transition represents a critical mechanical phenomenon wherein a material undergoes a fundamental transformation in its failure mode, transitioning from brittle fracture characteristics to ductile deformation behavior under applied stress conditions. At certain temperatures and pressures, the plasticity and toughness of a material depend on its crystal structure and the strength of atomic interactions. Specifically, the brittle-to-ductile transition is strongly correlated with the ratio between bulk modulus (*B*) and shear modulus (*G*), denoted as *B*/*G* [32]. This ratio is an effective indicator for predicting the material's toughness and brittleness behavior under different temperature or stress conditions. The *B*/*G* ratio serves as a critical indicator for material toughness, with the threshold value of 1.75 demarcating distinct mechanical behavior;: values exceeding

1.75 typically signify enhanced toughness and ductile characteristics, while ratios below this critical value are indicative of reduced toughness and increased brittleness [35]. As shown in Figure 6, as pressure gradually increases from 0 to 60 GPa, the *B/G* ratio exhibits a continuous upward trend, rising steadily from approximately 1.3 to nearly 1.7. This change indicates that under high-pressure conditions, the ability of Sc_3AlC to resist uniform compression (represented by the bulk modulus *B*) improves more significantly compared to its ability to resist shear deformation (represented by the shear modulus *G*). Within the pressure range of this study, the *B/G* ratio remains below 1.75 but gradually approaches this value with increasing pressure, suggesting that as pressure increases, Sc_3AlC tends to transition towards more toughness mechanical behavior while maintaining relative brittleness characteristics within the 0–60 GPa pressure range.

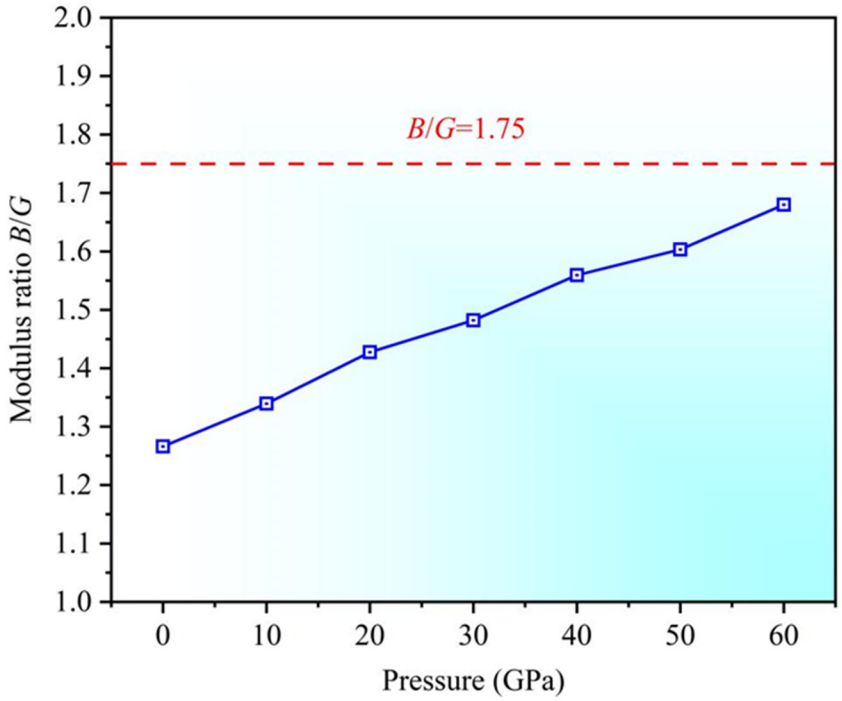

Figure 6. Variation curves depicting *B/G* versus applied pressure.

3.3. Anisotropy

Elastic anisotropy represents a fundamental physical parameter that plays a pivotal role in characterizing and understanding the mechanical behavior of crystalline materials with anisotropic characteristics, particularly in determining their directional dependence of elastic properties. The anisotropy of materials is often characterized using the anisotropy factor *A*, and a greater deviation of anisotropy factor *A* from the one indicates stronger anisotropy [36,37]. The cross-slip pinning model provides a theoretical framework for analyzing dislocation behavior, slip systems, and pinning effects in metallic materials [38]. It is particularly effective in analyzing the mechanisms of plastic deformation and their relationship with anisotropy factor. This model integrates the phenomena of cross-slip and pinning, enabling a more comprehensive understanding of stress transmission and dislocation glide in anisotropic materials. The anisotropy factor for the Sc_3AlC MAX phase can be calculated using the following formulas [39,40]:

$$A_{(100)[001]} = \frac{2C_{44}}{C_{11} - C_{12}} \quad (7)$$

$$A_{(110)[001]} = \frac{C_{44}(C' + 2C_{12} + C_{11})}{C_{11}C' - C_{12}^2} \tag{8}$$

where $C' = (C_{11} + C_{12})/2 + C_{44}$, and both $A_{(100)[001]}$ and $A_{(110)[001]}$ represent the anisotropy factors along the $(100)[001]$ and $(110)[001]$ crystallographic directions, respectively. According to Equations (7) and (8), Figure 7 illustrates the variation trends of anisotropy factors along the $(100)[001]$ direction (labeled as $A_{(100)[001]}$) and the $(110)[001]$ direction (labeled as $A_{(110)[001]}$) under increasing pressure. As the pressure rises from 0 to 60 GPa, both $A_{(100)[001]}$ and $A_{(110)[001]}$ exhibit a declining trend. This suggests that under high pressure, the degree of anisotropy in Sc_3AlC along these two directions gradually increases, and the differences in mechanical properties along these directions increase with increasing pressure. The pressure-dependent variation in the anisotropy factors reflects the rearrangement of atoms, including changes in interatomic distances. These factors lead to the gradual increases in the differences in mechanical responses along different crystallographic directions.

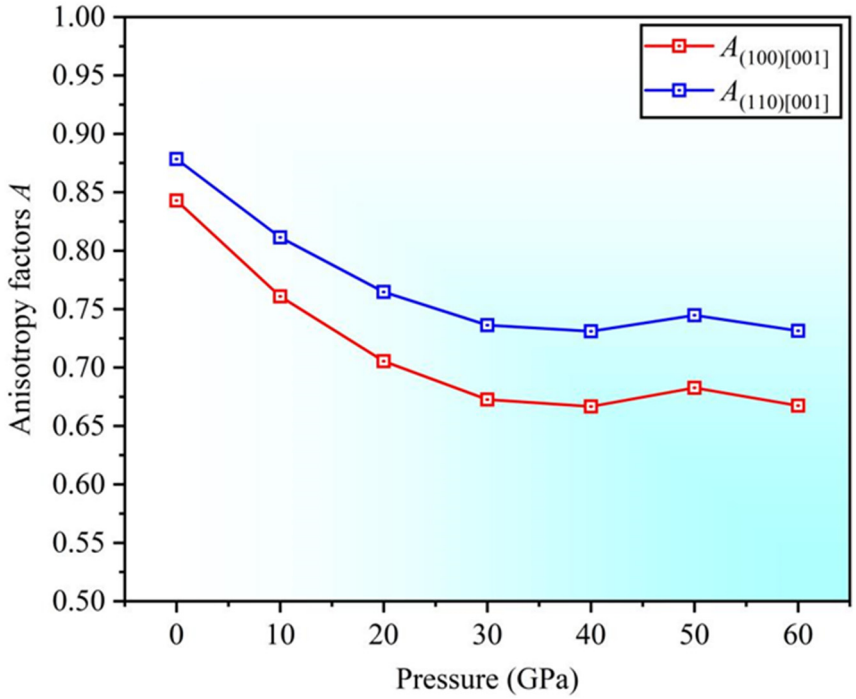

Figure 7. Variation curves depicting anisotropy factors A versus applied pressure.

Poisson's ratio σ is a physical quantity that describes the ratio of transverse strain to longitudinal strain when a material is subjected to tension or compression, typically ranging between 0 and 0.5. For different types of materials, Poisson's ratio is closely related to plasticity properties. According to Equations (9) and (10) [39,41], Figure 8 illustrates the variation trends of Poisson's ratio $\sigma_{[001]}$ in the [001] direction and $\sigma_{[111]}$ in the [111] direction under increasing pressure. In general, a large Poisson's ratio typically suggests good plasticity. At the initial stage, the Poisson ratio in both directions of the [001] and [111] is small, and with the increase of pressure, the Poisson ratio in both crystal directions increases, which indicates that the increase of pressure is conducive to improving the plasticity of the material. Furthermore, the value of $\sigma_{[111]}$ consistently exceeds that of $\sigma_{[001]}$ throughout the pressure range, suggesting that under the same pressure conditions, Sc3AlC exhibits better plasticity in the [111] direction compared to the [001] direction.

$$\sigma_{[001]} = \frac{C_{12}}{C_{11} + C_{12}} \tag{9}$$

$$\sigma_{[111]} = \frac{C_{11} + 2C_{12} - 2C_{44}}{2(C_{11} + 2C_{12} + C_{44})} \quad (10)$$

To further elucidate the evolution of the mechanical properties of Sc_3AlC under high pressure, other relevant properties are calculated within the pressure range of 0 to 60 GPa, with the variations illustrated in Figure 9. Figure 9 presents the trends of $C_{12} - C_{14}$ (representing the Cauchy pressure), $G_{(100)[010]}$ (shear modulus $G_{(100)[010]} = C_{44}$ in the $(100)[010]$ direction), $G_{(110)[1\bar{1}0]}$ (shear modulus $G_{(110)[1\bar{1}0]} = (C_{11} - C_{12})/2$ in the $(110)[1\bar{1}0]$ direction), and $E_{\langle 100\rangle}$ (Young's modulus in the <100> direction) as functions of pressure, where $E_{\langle 100\rangle}$ is expressed by $E_{\langle 100\rangle} = (C_{11} - C_{12})[1 + C_{12}/(C_{11} + C_{12})]$ [42,43]. As the pressure increases from 0 GPa to 60 GPa, $E_{\langle 100\rangle}$ exhibits a significant upward trend, steadily rising from its initial value to a high level, which indicates that under high pressure, the ability of Sc_3AlC to resist elastic deformation in the <100> direction is significantly enhanced, with the interatomic bonding forces in this direction markedly increasing with pressure. Both $G_{(100)[010]}$ and $G_{(110)[1\bar{1}0]}$ also increase with increasing pressure, although their growth rates are relatively smaller compared to $E_{\langle 100\rangle}$. This suggests that in a high-pressure environment, the resistance of Sc_3AlC to shear deformation in these two directions is improved. Generally, a negative Cauchy pressure indicates that the material possesses directional bonding characteristics, and a positive Cauchy pressure suggests metallic characteristic [43–45]. The Cauchy pressure $C_{12} - C_{14}$ remains negative throughout the pressure range; however, it gradually increases and asymptotically approaches zero as the pressure rises. This trend indicates a weakening of the directional characteristics of interatomic bonding within the material, accompanied by an enhancement of metallic properties.

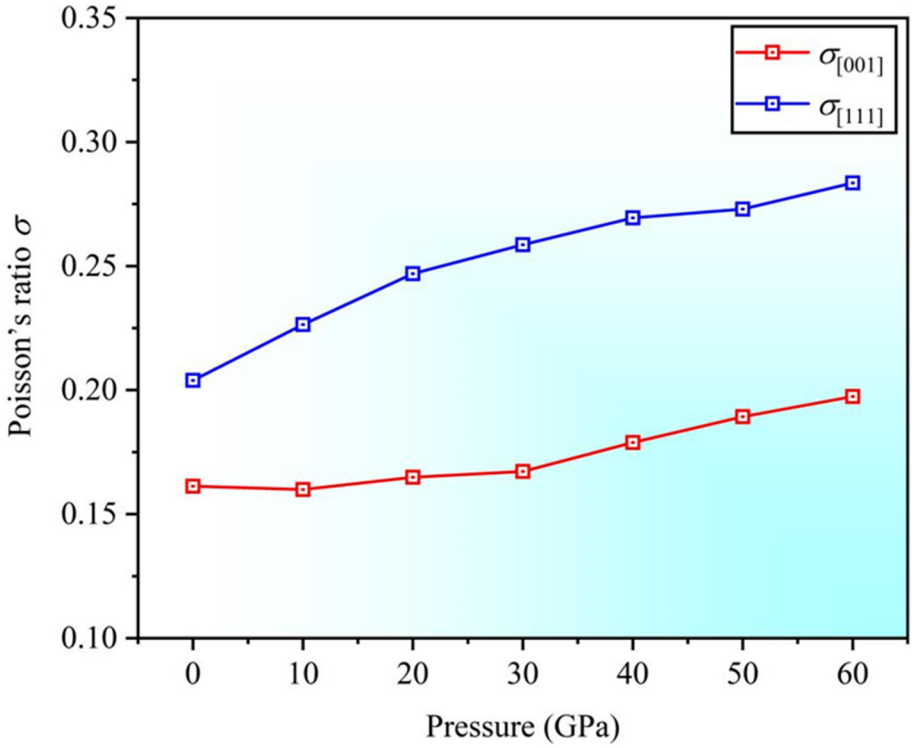

Figure 8. Variation curves depicting Poisson's ratio σ versus applied pressure.

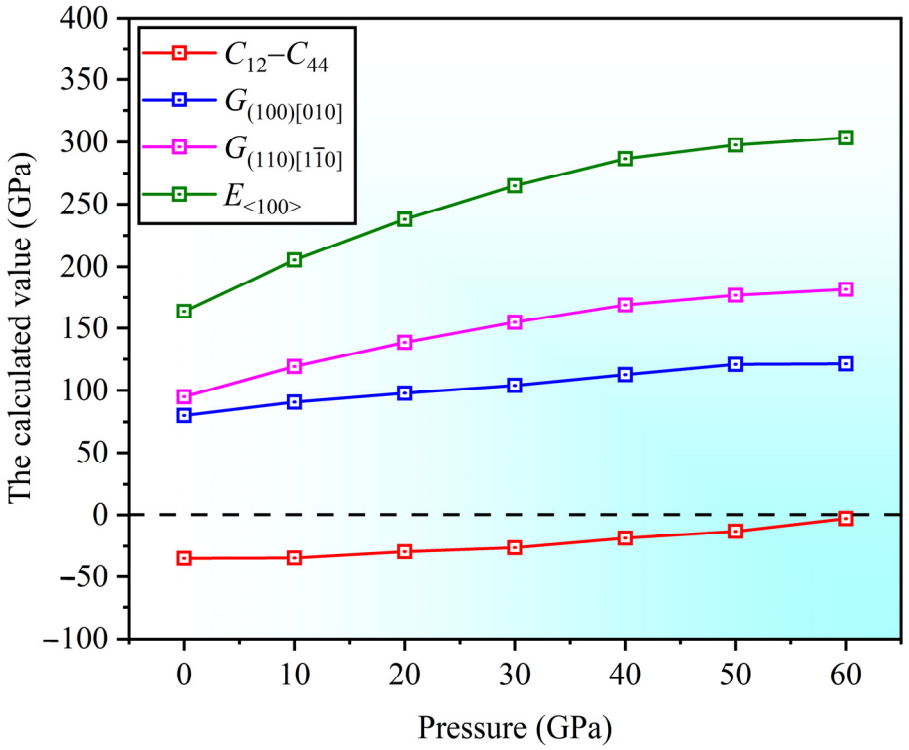

Figure 9. Variation curves depicting Cauchy pressure and material modulus versus applied pressure.

3.4. Hardness and Yield Strength

Hardness and yield strength are essential parameters for characterizing a material's resistance to deformation, and they are closely related to the material's mechanical properties [46]. Specifically, hardness is defined as the ability of a material's surface to resist localized plastic deformation, such as indentation, scratching, or wear. An increased hardness value implies that the material is less susceptible to plastic deformation. On the other hand, yield strength σ_y is defined as the minimum stress where a material begins to undergo permanent deformation during tension or compression. Once the applied stress exceeds the yield strength, the material translates from elastic to plastic deformation. Previous studies [47–50] indicate that the Vickers hardness (H_V) of a material can be determined using Equation (11), where $k = G/B$ [51]. The Vickers hardness (H_V) is approximately three times yield strength (σ_y), as expressed in Equation (12).

To explore the effects of high pressure on the Vickers hardness and yield strength of Sc_3AlC, the relevant data are calculated within the pressure range of 0 to 60 GPa, as illustrated in Figure 10. Figure 10a shows the variation of Vickers hardness versus applied pressure, while Figure 10b presents the changes in yield strength under pressure. From Figure 10a, the value of Vickers hardness is about 17.52 GPa at ambient pressure, aligning well with the calculated result (H_V = 17.81 GPa) of Rayhan et al. [26], and it can be observed that within the pressure range of 0 to 10 GPa, the Vickers hardness increases rapidly from approximately 17.52 GPa to about 18.16 GPa. This indicates that during the initial stage of pressure increase, the resistance to localized plastic deformation significantly improves in the Sc_3AlC MAX phase. Subsequently, from 10 GPa to 50 GPa, H_V fluctuates within the range of 17.52 GPa to 18.16 GPa, remaining relatively stable. This suggests that changes in pressure have a minimal impact on Vickers hardness of Sc_3AlC phase. However, when the pressure exceeds 50 GPa, H_V drops sharply, reaching approximately 16.84 GPa at P = 60 GPa, which demonstrates that the hardness value decreases significantly under high pressure. In Figure 10b, the yield strength shows an increase from 5.84 GPa to 6.05 GPa within the 0 to 10 GPa range, indicating that the stress to resist plastic deformation increases.

From 10 GPa to 50 GPa, σ_y fluctuates between 5.84 GPa and 6.05 GPa, remaining relatively stable, which suggests that the yield characteristics of the material are relatively stable within this pressure range. However, when the pressure reaches 60 GPa, σ_y decreases to about 5.61 GPa, indicating a reduction in the material's yield strength under the conditions of high pressure.

$$H_v = 2\left(k^2 G\right)^{0.585} - 3 \tag{11}$$

$$\sigma_y = H_V/3 \tag{12}$$

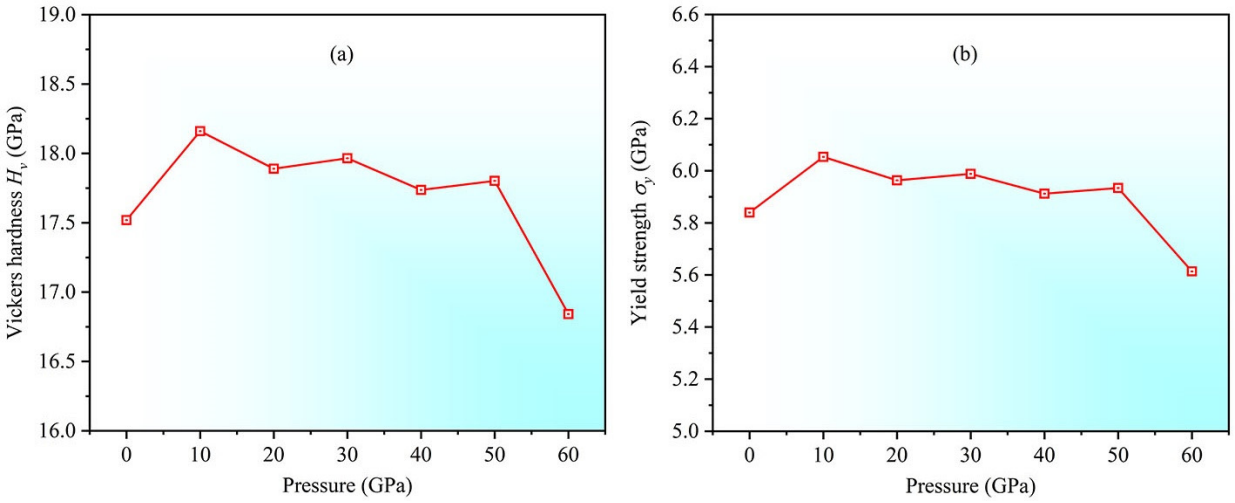

Figure 10. Variation curves depicting H_V (**a**) and σ_y (**b**) versus applied pressure.

3.5. Energy Factor K

In crystalline materials, the ability of dislocation nucleation is closely associated with the material's plasticity. The energy factor K is a crucial parameter that quantifies the dislocation nucleation ability, representing the minimum energy for plastic deformation in a specific direction, and the calculation of energy factor K is related to the elastic constant. For cubic crystals, Equations (13) and (14) give the expressions of K factors of edge and screw dislocations [52,53]. Based on the calculated results, Figure 11 illustrates the variation of the energy factor K for edge and screw dislocations versus applied pressure. As the pressure increases from 0 to 60 GPa, the energy factors K for both edge and screw dislocations increase. For edge dislocations, the energy factor K_{edge} increases steadily from an initial value of 107.45 GPa to 197.68 GPa, which suggests that under high-pressure conditions, the nucleation energy of edge dislocations in Sc_3AlC significantly increases, resulting in a higher energy barrier that must be overcome for dislocation nucleation, thereby inhibiting plastic deformation. For screw dislocations, the energy factor K_{screw} gradually rises from 87.22 GPa to 148.38 GPa, indicating that the nucleation energy also increases with increasing pressure, thus leading to the inhibition of screw dislocations.

$$K_{\text{screw}} = \left[\frac{1}{2}C_{44}(C_{11} - C_{12})\right]^{\frac{1}{2}} \tag{13}$$

$$K_{\text{edge}} = (C_{11} + C_{12})\left[\frac{(C_{11} - C_{12})C_{44}}{(C_{11} + C_{12} + 2C_{44})C_{11}}\right]^{\frac{1}{2}} \tag{14}$$

The mixed dislocation factor K_{mixed} is a parameter that quantifies the nucleation of mixed dislocations, and this factor can be characterized as a function of the orientation angle θ. For mixed dislocations, the dislocation core width ζ represents the extent of deformation within the dislocation region. The relationships between K_{mixed}, ζ, and other

parameters are described by Equations (15) and (16) [53,54], where $C = (C_{11} - C_{12})/2$, with d denoting the distance between adjacent slip planes. Figure 12 shows the calculated curves of K_{mixed} and ζ versus applied pressure. In Figure 12a, as pressure increases, the mixed dislocation factor K_{mixed} also increases, which is consistent with the conclusion in Figure 11. In Figure 12b, it is evident that the dislocation core width gradually decreases as pressure increases, which increases the stacking-fault energy of the Sc_3AlC MAX phase, and then inhibits twinning deformation.

$$K_{\mathrm{mixed}} = K_{\mathrm{edge}} \cdot \sin^2\theta + K_{\mathrm{screw}} \cdot \cos^2\theta \tag{15}$$

$$\zeta = \frac{K_{\mathrm{mixed}} \cdot d}{2C} \tag{16}$$

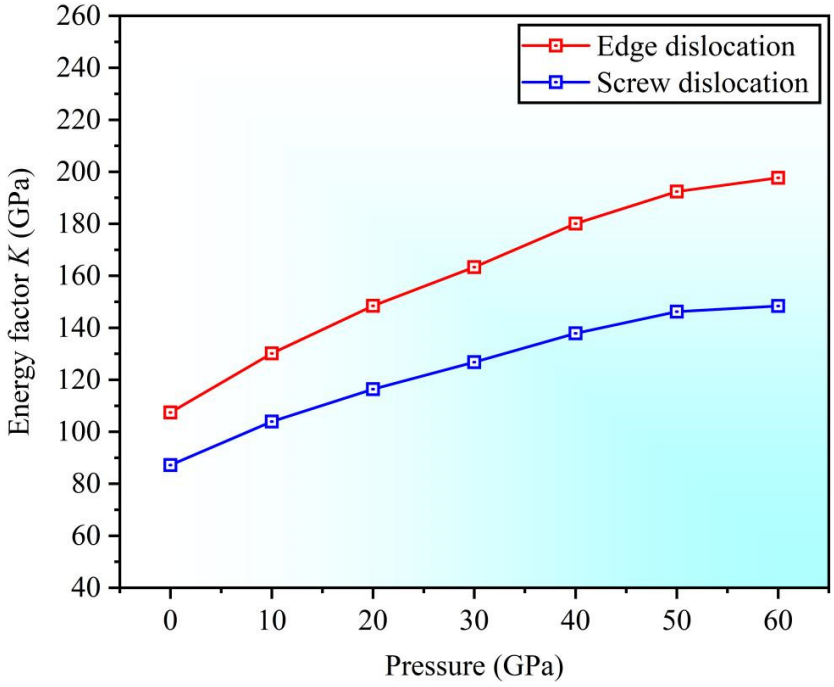

Figure 11. Variation curves depicting energy factors K for screw and edge dislocations versus applied pressure.

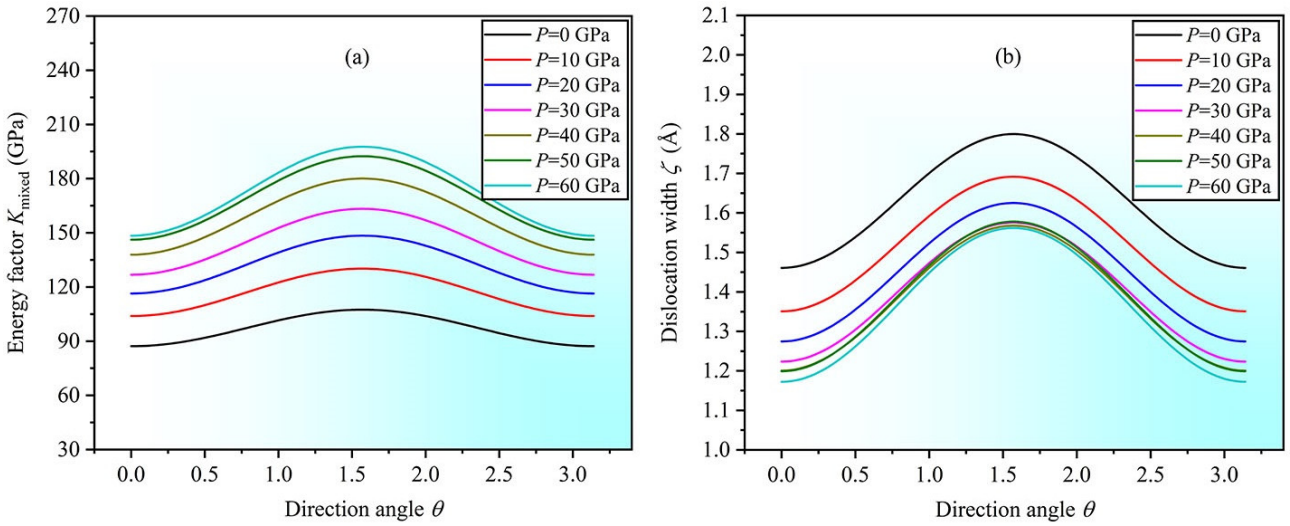

Figure 12. Variation curves depicting K_{mixed} factor of mixed dislocation (**a**) and dislocation width ζ (**b**) versus direction angle $\theta(0 \leq \theta \leq \pi)$ at various pressures.

3.6. Electronic Properties

The electronic structure is intrinsically related to the bonding mechanisms and directly affects the structural stability of a material. To examine the effects of high pressure on the electronic structure of Sc_3AlC, the variation of total density of states (TDOS) is analyzed under pressures ranging from 0 to 60 GPa, as shown in Figure 13. As the pressure increases from 0 to 60 GPa, the TDOS at the Fermi level slightly increases, and the DOS for both the valence and conduction bands near the Fermi level shifts slightly to the right, indicating that high pressure enhances the interatomic bonding in the Sc_3AlC MAX phase, while the enhancement effect is not substantial.

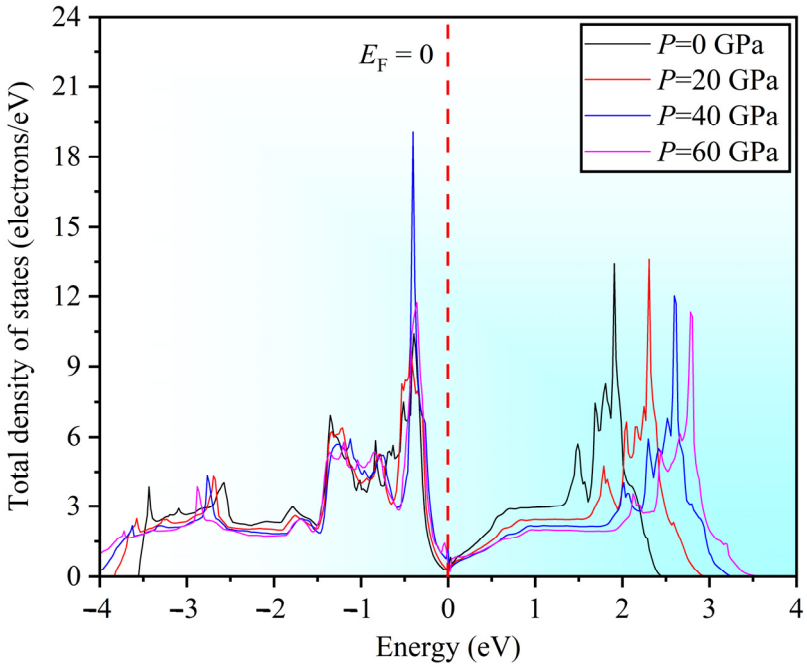

Figure 13. TDOS of Sc_3AlC MAX phase under different pressures.

4. Conclusions

This work systematically investigates the effects of pressure on the structural, mechanical, dislocation, and electronic properties of the Sc_3AlC MAX phase using first-principles calculations. The main conclusions are as follows:

(1) Under pressures ranging from 0 to 60 GPa, the lattice constant ratio and volume ratio decrease. The elastic constants satisfy stability criteria, indicating that the structure remains stable under high pressure.

(2) As the pressure increases, the bulk modulus, Young's modulus, and shear modulus increase, enhancing resistance to material deformation. The B/G ratio rises, approaching 1.75, suggesting a tendency toward ductile behavior, but the material still maintains its brittle characteristics.

(3) As the pressure increases, the anisotropy in the $(100)[001]$ and $(110)[001]$ directions also increases. The Poisson's ratio in the [001] and [111] directions increases, resulting in the enhanced plasticity, with better plasticity along the [111] direction. The negative Cauchy pressure indicates the directional characteristics of interatomic bonding.

(4) Vickers hardness and yield strength increase under pressures of 0 to 10 GPa and remain relatively stable between 10 and 50 GPa, and then decrease sharply above 50 GPa.

(5) High pressure increases the energy factors of edge and screw dislocations, suppressing dislocation nucleation. The mixed dislocation factor increases with increasing pressure, and the dislocation core width reduces, which may inhibit twinning deformation.
(6) High pressure enhances the interatomic bonding in the Sc_3AlC MAX phase, while the enhancement effect is not substantial.

Author Contributions: Methodology, Formal analysis, Investigation, Writing—original draft, J.X., Z.W. and L.Z.; Funding acquisition, Supervision, Visualization, Z.W. and L.M.; Project administration, Data curation, L.Z.; Software, P.T.; Writing—review and editing, J.X., Z.W. and L.M. All authors have read and agreed to the published version of the manuscript.

Funding: This research was funded by the National Natural Science Foundation of China (52162009), State Key Laboratory of Advanced Design and Manufacturing for Vehicle Body, Hunan University, Changsha, China (32175006).

Data Availability Statement: The data presented in this study are available on request from the corresponding authors.

Conflicts of Interest: The authors declare no conflicts of interest.

References

1. Dong, H.; Yu, Y.; Jin, X.; Tian, X.; He, W.; Ma, W. Microstructure and mechanical properties of SiC-SiC joints joined by spark plasma sintering. *Ceram. Int.* **2016**, *42*, 14463–14468. [CrossRef]
2. Shrivastava, V. Microwave processed $SrBi_2Nb_2O_9$ ferroelectric ceramics with controlled dielectric relaxation and metallic conduction. *Ceram. Int.* **2016**, *42*, 10122–10126. [CrossRef]
3. Lu, Y.; Yang, A.; Duan, Y.; Peng, M. Structural stability, electronic and optical properties of MAX-phase ternary nitrides β-TM_4AlN_3 (TM = V, Nb, and Ta) using the first-principles explorations. *Vacuum* **2021**, *193*, 110529. [CrossRef]
4. Zhang, Z.; Duan, X.; Jia, D.; Zhou, Y.; Zwaag, S.V.D. On the formation mechanisms and properties of MAX phases: A review. *J. Eur. Ceram. Soc.* **2021**, *41*, 3851–3878. [CrossRef]
5. Ching, W.Y.; Mo, Y.; Aryal, S.; Rulis, P. Intrinsic mechanical properties of 20 MAX-phase compounds. *J. Am. Ceram. Soc.* **2013**, *96*, 2292–2297. [CrossRef]
6. Sokol, M.; Natu, V.; Kota, S.; Barsoum, M.W. On the chemical diversity of the MAX phases. *Trends Chem.* **2019**, *1*, 210–223. [CrossRef]
7. Sauceda, D.; Singh, P.; Falkowski, A.; Chen, Y.; Doung, T.; Vazquez, G.; Radovic, M.; Arroyave, R. High-throughput reaction engineering to assess the oxidation stability of MAX phases. *NPJ Comput. Mater.* **2021**, *7*, 6. [CrossRef]
8. Badie, S.; Sebold, D.; Vaßen, R.; Guillon, O.; Gonzalez-Julian, J. Mechanism for breakaway oxidation of the Ti_2AlC MAX phase. *Acta Mater.* **2021**, *215*, 117025. [CrossRef]
9. Bao, W.; Wang, X.G.; Ding, H.; Lu, P.; Zhu, C.; Zhang, G.J.; Xu, F. High-entropy M_2AlC-MC (M = Ti, Zr, Hf, Nb, Ta) composite: Synthesis and microstructures. *Scripta Mater.* **2020**, *183*, 33–38. [CrossRef]
10. Nowotny, H.; Boller, H.; Beckmann, O. Alloy phases crystallizing with structures which occur with nonmetallic compounds. *J. Solid State Chem.* **1970**, *2*, 462–471. [CrossRef]
11. Nowotny, V.H. Strukturchemie einiger verbindungen der übergangsmetalle mit den elementen C, Si, Ge, Sn. *Prog. Solid State Chem.* **1971**, *5*, 27–70. [CrossRef]
12. Ghule, A.; Ghule, S.; Garde, C.; Pandey, B.; Ramakrishnan, S. Ab initio study of Sc_3MO (M = Al, Ga, In, Tl) and systematics in Sc_3MZ (Z = B, C, N, O). *Comput. Condens. Matter* **2020**, *25*, e00509. [CrossRef]
13. Chern, M.Y.; Vennos, D.; DiSalvo, F. Synthesis, structure, and properties of anti-perovskite nitrides Ca_3MN, M = P, As, Sb, Bi, Ge, Sn, and Pb. *J. Solid State Chem.* **1992**, *96*, 415–425. [CrossRef]
14. Deng, Z.; Ni, D.; Chen, D.; Bian, Y.; Li, S.; Wang, Z.; Zhao, Y. Anti-perovskite materials for energy storage batteries. *InfoMat* **2022**, *4*, e12252. [CrossRef]
15. Lenggenhager, P.M.; Liu, X.; Neupert, T.; Bzdušek, T. Universal higher-order bulk-boundary correspondence of triple nodal points. *Phys. Rev. B* **2022**, *106*, 085129. [CrossRef]
16. Kresse, G.; Furthmüller, J. Efficient iterative schemes for ab initio total-energy calculations using a plane-wave basis set. *Phys. Rev. B* **1996**, *54*, 11169–11186. [CrossRef]
17. Kresse, G.; Hafner, J. Ab initio molecular dynamics for liquid metals. *Phys. Rev. B* **1993**, *47*, 558–561. [CrossRef]
18. Blöchl, P.E. Projected augmented-wave method. *Phys. Rev. B* **1994**, *50*, 17953–17979. [CrossRef]

19. Perdew, J.P.; Burke, K.; Wang, Y. Generalized gradient approximation for the exchange-correlation hole of a many-electron system. *Phys. Rev. B* **1996**, *54*, 16533. [CrossRef]
20. Pack, J.D.; Monkhorst, H.J. Special Points for Brillonin-Zone Integrations. *Phys. Rev. B* **1976**, *13*, 5188.
21. Birch, F. Finite elastic strain of cubic crystals. *Phys. Rev.* **1947**, *71*, 809. [CrossRef]
22. Gesing, T.M.; Wachtmann, K.H.; Jeitschko, W. The Perovskite Carbides A_3MC (A = Sc, Y, La-Nd, Sm, Gd-Lu; M = AI, Ga, In, Tl, Sn, Pb). *Z. Naturforsch. B* **1997**, *52*, 176–182. [CrossRef]
23. Haddadi, K.; Bouhemadou, A.; Zerarga, F.; Bin-Omran, S. First-principles investigation of the ternary scandium based inverse-perovskite carbides Sc_3AC (A = Al, Ga, In and Tl). *Solid State Sci.* **2012**, *14*, 1175–1185. [CrossRef]
24. Kanchana, V.; Ram, S. Electronic structure and mechanical properties of Sc_3AC (A = Al, Ga, In, Tl) and Sc_3BN (B = Al, In): Ab-initio study. *Intermetallics* **2012**, *23*, 39–48. [CrossRef]
25. Medkour, Y.; Roumili, A.; Maouche, D.; Saoudi, A. A first-principles study on the structural, elastic and electronic properties of $AlCSc_3$ and $AlNSc_3$. *Solid State Commun.* **2009**, *149*, 1840–1842. [CrossRef]
26. Rayhan, M.; Ali, M.; Jahan, N.; Hossain, M.; Uddin, M.; Islam, A.; Naqib, S. Insights into the unrevealed physical properties of $Sc_2Al_2C_3$ compared with other Sc-Al-C systems via ab-initio investigation. *Phys. Open* **2024**, *19*, 100217. [CrossRef]
27. Wang, K.; Zhang, X.; Wang, F. Exploring the electronic, mechanical, anisotropic and optical properties of the Sc-Al-C MAX phases from a first principles calculations. *Chem. Phys. Lett.* **2024**, *836*, 141024. [CrossRef]
28. Patil, S.K.R.; Khare, S.V.; Tuttle, B.R.; Bording, J.K.; Kodambaka, S. Mechanical stability of possible structures of PtN investigated using first-principles calculations. *Phys. Rev. B* **2006**, *73*, 104118. [CrossRef]
29. Wang, J.; Yip, S.; Phillpot, S.R.; Wolf, D. Crystal instabilities at finite strain. *Phys. Rev. Lett.* **1993**, *71*, 4182. [CrossRef]
30. Wallace, D.C.; Callen, H. Thermodynamics of Crystals. *Am. J. Phys.* **1972**, *40*, 1718–1719. [CrossRef]
31. Yang, X.W.; Zhu, J.C.; Lai, Z.H.; Liu, Y.; He, D.; Nong, Z.S. Finite element analysis of quenching temperature field, residual stress and distortion in A357 aluminum alloy large complicated thin-wall workpieces. *T. Nonferr. Metal. Soc.* **2013**, *23*, 1751–1760. [CrossRef]
32. Lu, Y.; Yang, Y.; Zheng, F.; Wang, B.T.; Zhang, P. Electronic, mechanical, and thermodynamic properties of americium dioxide. *J. Nucl. Mater.* **2013**, *441*, 411–420. [CrossRef]
33. Hill, R. The elastic behavior of crystalline aggregate. *Proc. Phys. Soc. A* **1952**, *65*, 349–354. [CrossRef]
34. Iotova, D.; Kioussis, N.; Lim, S.P. Electronic structure and elastic properties of the Ni_3X (X = Mn, Al, Ga, Si, Ge) intermetallics. *Phys. Rev. B* **1996**, *54*, 14413–14422. [CrossRef] [PubMed]
35. Cottrel, A.H. Advanced Structural Materials. In Proceedings of the 2nd European Conference on Advanced Materials and Processes, Cambridge, UK, 22–24 July 1991.
36. Fu, H.; Li, D.; Peng, F.; Gao, T.; Cheng, X. Structural and elastic properties of γTiAl under high pressure from electronic structure calculations. *J. Alloys Comp.* **2009**, *473*, 255–261. [CrossRef]
37. Mattesini, M.; Ahuja, R.; Johansson, B. Cubic Hf_3N_4 and Zr_3N_4: A class of hard materials. *Phys. Rev. B* **2003**, *68*, 184108. [CrossRef]
38. Yoo, M.H. On the theory of anomalous yield behavior of Ni_3Al—Effect of elastic anisotropy. *Scripta Metall.* **1986**, *20*, 915–920. [CrossRef]
39. Fu, H.; Li, X.F.; Liu, W.F.; Ma, Y.; Tao, G.; Hong, X. Electronic and dynamical properties of NiAl studied from first principles. *Intermetallics* **2011**, *19*, 1959–1967. [CrossRef]
40. Lau, K.; McCurdy, A.K. Elastic anisotropy factors for orthorhombic, tetragonal, and hexagonal crystals. *Phys. Rev. B* **1998**, *58*, 8980–8984. [CrossRef]
41. Friák, M.; Šob, M.; Vitek, V. Ab initio calculation of tensile strength in iron. *Philos. Mag.* **2003**, *83*, 3529–3537. [CrossRef]
42. Zhu, Y.M.; Weyland, M.; Morton, A.J.; Oh-ishi, K.; Hono, K.; Nie, J.F. The building block of long-period structures in Mg-RE-Zn alloys. *Scripta Mater.* **2009**, *60*, 980–983. [CrossRef]
43. Fu, H.; Li, D.; Peng, F.; Gao, T.; Cheng, X. Ab initio calculations of elastic constants and thermodynamic properties of NiAl under high pressures. *Comp. Mater. Sci.* **2008**, *44*, 774–778. [CrossRef]
44. Johnson, R.A. Analytic nearest-neighbor model for fcc metals. *Phys. Rev. B* **1988**, *37*, 3924–3931. [CrossRef]
45. Pettifor, D. Theoretical predictions of structure and related properties of intermetallics. *Mater. Sci. Technol.* **1992**, *8*, 345–349. [CrossRef]
46. Tse, J.S. Intrinsic hardness of crystalline solids. *J. Superhard Mater.* **2010**, *32*, 177–191. [CrossRef]
47. Smedskjaer, M.M.; Mauro, J.C.; Yue, Y. Prediction of glass hardness using temperature-dependent constraint theory. *Phys. Rev. Lett.* **2010**, *105*, 115503. [CrossRef]
48. Li, K.; Wang, X.; Zhang, F.; Xue, D. Electronegativity identification of novel superhard materials. *Phys. Rev. Lett.* **2008**, *100*, 235504. [CrossRef] [PubMed]
49. Gao, F.; He, J.; Wu, E.; Liu, S.; Yu, D.; Li, D.; Zhang, S.; Tian, Y. Hardness of covalent crystals. *Phys. Rev. Lett.* **2003**, *91*, 015502. [CrossRef]

50. Šimůnek, A.; Vackář, J. Hardness of covalent and ionic crystals: First-principle calculations. *Phys. Rev. Lett.* **2006**, *96*, 085501. [CrossRef]
51. Chen, X.; Niu, H.; Li, D.; Li, Y. Modeling hardness of polycrystalline materials and bulk metallic glasses. *Intermetallics* **2011**, *19*, 1275–1281. [CrossRef]
52. Savin, M.M.; Chernov, V.M.; Strokova, A.M. Energy factor of dislocations in hexagonal crystals. *Phys. Status Solidi A* **1976**, *35*, 747–754. [CrossRef]
53. Foreman, A.J.E. Dislocation energies in anisotropic crystals. *Acta Metall.* **1955**, *3*, 322–330. [CrossRef]
54. Reid, C.N. Dislocation widths in anisotropic B.C.C. crystals. *Acta Metall.* **1966**, *14*, 13–16. [CrossRef]